Quantum Electrodynamics and Quantum Optics: Lecture 6

Fall 2025

Ill. Niklas Elmehed © Nobel Prize Outreach

John Clarke

Prize share: 1/3

Ill. Niklas Elmehed © Nobel Prize Outreach

Michel H. Devoret

Prize share: 1/3

Ill. Niklas Elmehed © Nobel Prize Outreach

John M. Martinis

Prize share: 1/3

The Nobel Prize in Physics 2025 was awarded jointly to John Clarke, Michel H. Devoret and John M. Martinis "for the discovery of macroscopic quantum mechanical tunnelling and energy quantisation in an electric circuit"

Measurements of Macroscopic Quantum Tunneling out of the Zero-Voltage State of a Current-Biased Josephson Junction

Michel H. Devoret,[a] John M. Martinis, and John Clarke
Department of Physics, University of California, Berkeley, California 94720, and Materials and Molecular Research Division, Lawrence Berkeley Laboratory, Berkeley, California 94720
(Received 26 July 1985)

The escape rate of an underdamped ($Q \approx 30$), current-biased Josephson junction from the zero-voltage state has been measured. The relevant parameters of the junction were determined *in situ* in the thermal regime from the dependence of the escape rate on bias current and from resonant activation in the presence of microwaves. At low temperatures, the escape rate became independent of temperature with a value that, with no adjustable parameters, was in excellent agreement with the zero-temperature prediction for macroscopic quantum tunneling.

PACS numbers: 74.50.+r, 03.65.−w, 05.30.−d, 05.40.+j

Quantum Mechanics of a Macroscopic Variable: The Phase Difference of a Josephson Junction

John Clarke, Andrew N. Cleland, Michel H. Devoret, Daniel Esteve, John M. Martinis

Experiments to investigate the quantum behavior of a macroscopic degree of freedom, namely the phase difference across a Josephson tunnel junction, are described. The experiments involve measurements of the escape rate of the junction from its zero voltage state. Low temperature measurements of the escape rate for junctions that are either nearly undamped or moderately damped agree very closely with predictions for macroscopic quantum tunneling, with no adjustable parameters. Microwave spectroscopy reveals quantized energy levels in the potential well of the junction in excellent agreement with quantum-mechanical calculations. The system can be regarded as a "macroscopic nucleus with wires."

emphasized, one must distinguish carefully between macroscopic quantum phenomena originating in the superposition of a large number of microscopic variables and those displayed by a single macroscopic degree of freedom. It is the latter that we discuss in this article.

Our usual observations on a billiard ball or Brownian particle reveal classical behavior because Planck's constant $\hbar$ is so tiny. However, at least in principle there is nothing to prevent us from designing an experiment in which these objects are quantum mechanical. To do so we have to satisfy two criteria: (i) the thermal energy must be small compared with the separation of the quantized energy levels, and (ii) the macroscopic degree of freedom must be sufficiently decoupled from all other degrees of freedom if the lifetime of the quantum states is to be longer than the characteristic time scale of the system (*1*). To illustrate the application of these

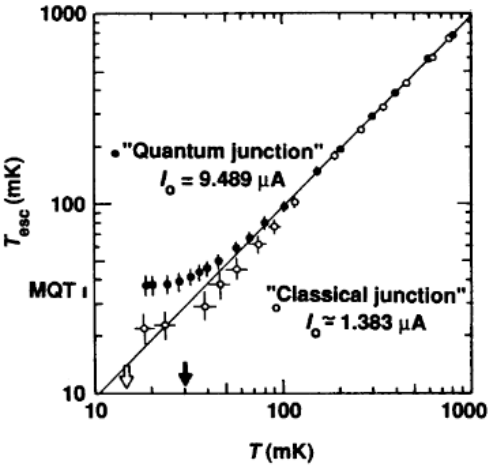

Fig. 4. T_{esc} versus T at $\ell n(\omega_p/2\pi\Gamma) = 11$ for the high and low values of I_0 with arrows indicating T_{cr} (solid and open circles and arrows). The vertical bar labeled MQT is the prediction for $I_0 = 9.489$ μA. The line is the thermal prediction $T_{esc} = 0.95T$. Horizontal error bars are a combination of systematic and random errors in the temperature scale; vertical error bars indicate primarily systematic uncertainties in the junction parameters. For clarity, error bars for T have been shown for the "classical junction" only; identical errors apply to the "quantum junction."

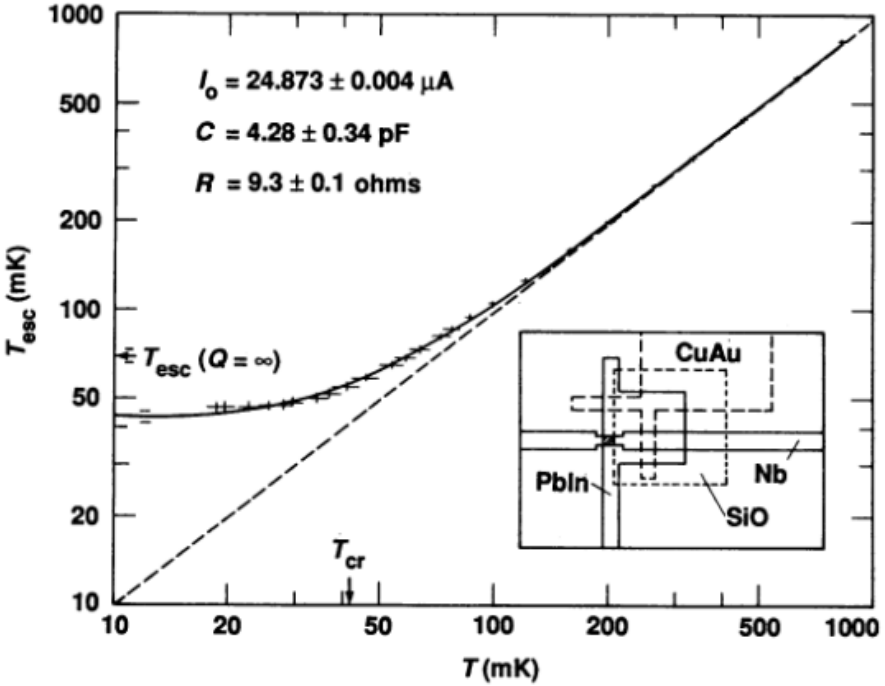

Fig. 5. T_{esc} versus T for shunted junction (configuration shown in inset). Solid curve is theory, dashed line is classical prediction $T_{esc} = 0.98T$. The crossover temperature T_{cr} for this junction and T_{esc} for $Q = \infty$ are indicated by arrows. Error bars are as in Fig. 4.

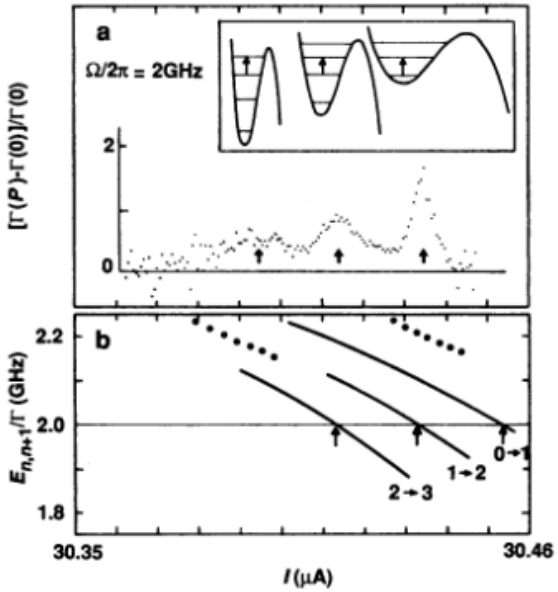

Fig. 6. (**a**) $[\Gamma(P) - \Gamma(0)]/\Gamma(0)$ versus I for an 80 by 10 μm^2 junction at 28 mK in the presence of 2.0 GHz microwaves ($k_B T/\hbar\Omega = 0.29$). Arrows indicate values of current at which the peaks of the resonances occur. Inset represents the corresponding transitions between energy levels. (**b**) Calculated energy-level spacings $E_{n,n+1}$ versus I for $I_0 = 30.572 \pm 0.017$ μA and $C = 47.0 \pm 3.0$ pF. Dotted lines indicate uncertainties in the $0 \rightarrow 1$ curve that arise from uncertainties in I_0 and C. Arrows indicate values of bias current at which resonances are predicted to occur.

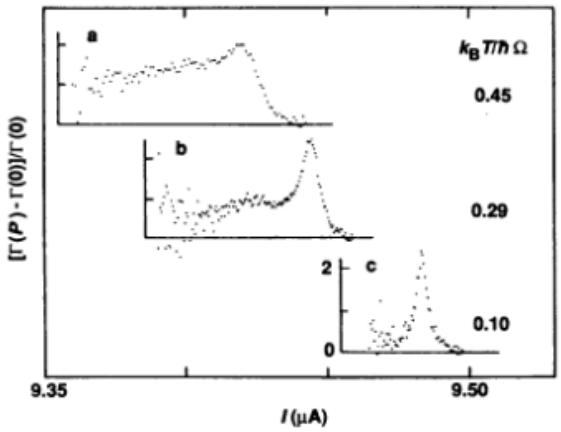

Fig. 7. $[\Gamma(P) - \Gamma(0)]/\Gamma(0)$ versus I for a 10 by 10 μm^2 junction with $I_0 \approx 9.57$ μA and $C \approx 6.35$ pF at three values of $k_B T/\hbar\Omega$. The microwave frequencies are: curve a, 4.5 GHz; curve b, 4.1 GHz; and curve c, 3.7 GHz.

Superconducting circuits

- Josephson Junctions
  - Current phase relationship
  - AC Josephson effect
- The cooper pair box (CPB)
  - Hamiltonian
  - Eigen-energies
  - Mathieu equation
  - Josephson Junctions Phase and Cooper pair box Number operator
- Cooper pair box and Transmon
  - Charge dispersion as a ratio of E_J and E_C
  - Anharmonicity
- Quantizing electrical circuits
  - Normal modes
  - Harmonic oscillator approximation

References: Implementatin of a superconducting qubit, Cottet, PhD Thesis

Josephson Junctions

References: Implementatin of a superconducting qubit, Cottet, PhD Thesis

Josephson junctions

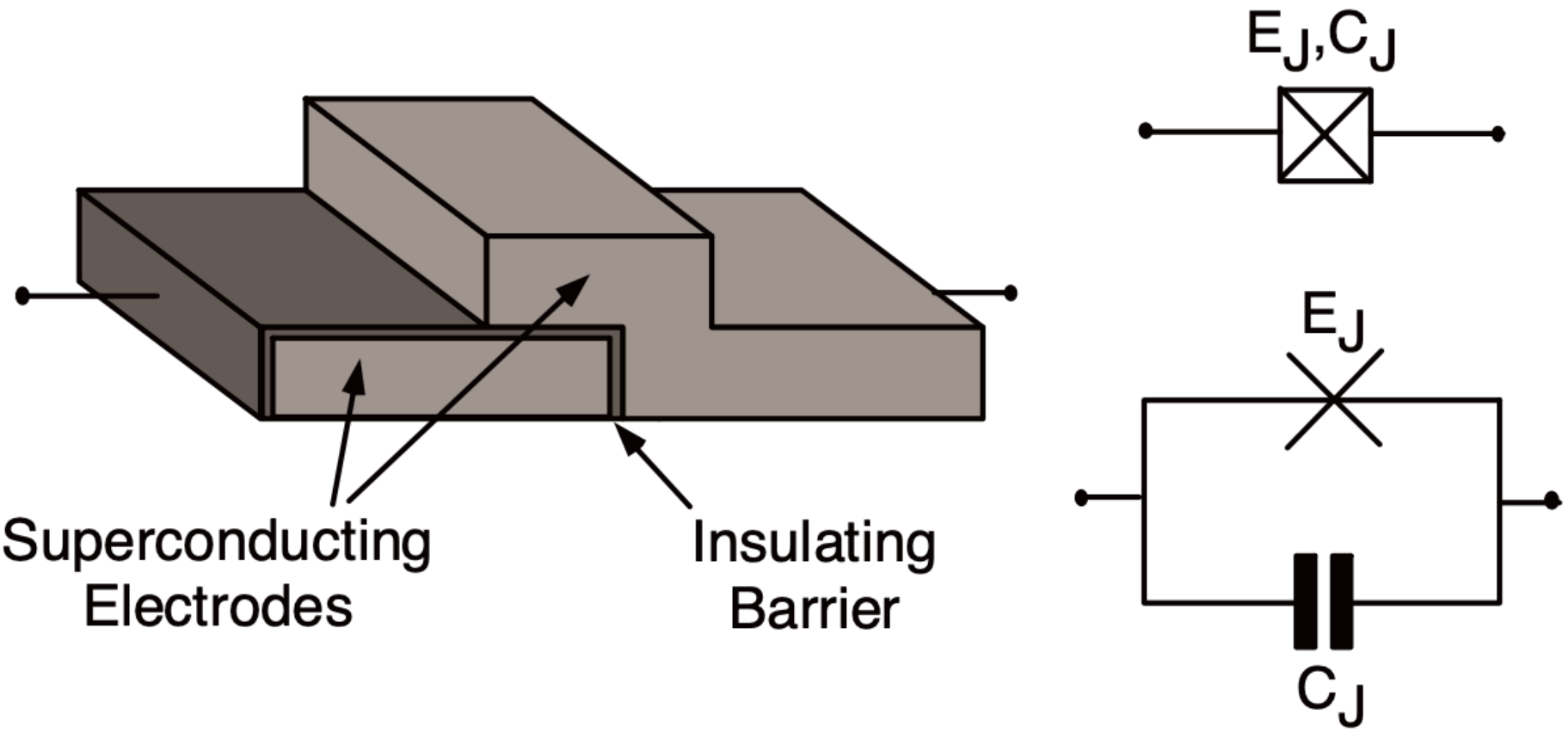

Left: Sketch of a Josephson junction. Top Right: Electrical symbol.

References: Implementation of a superconducting qubit, Cottet, PhD Thesis

Josephson junctions

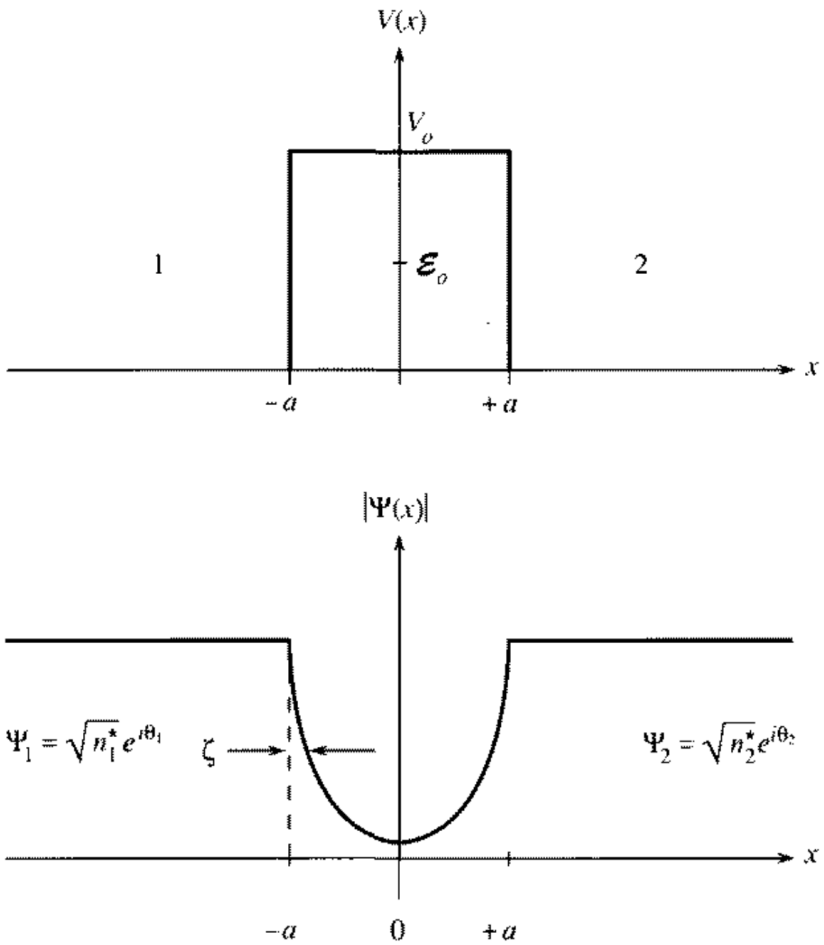

Figure 8.5 The model potential of the insulator $V(x)$ and the magnitude of the wavefunction $|\Psi|$. The two superconductors have densities of superconducting electron pairs n_1^* and n_2^*, respectively. Furthermore, the phase of the wavefunction θ can be different for the two superconductors at $x = \pm a$.

THE DISCOVERY OF TUNNELLING SUPERCURRENTS

Nobel Lecture, December 12, 1973

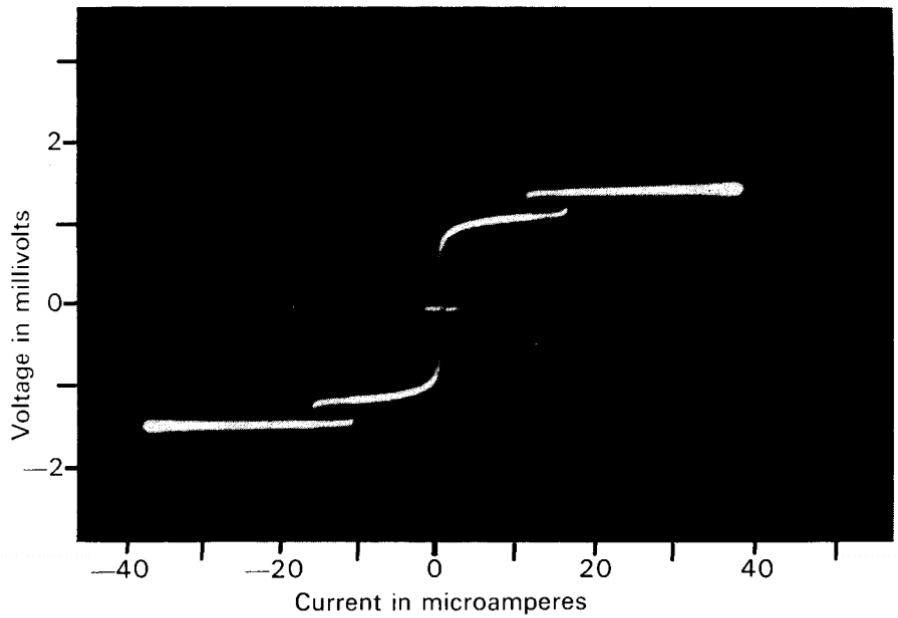

Fig. 3. The first published observation of tunnelling between two evaporated-film superconductors (Nicol, Shapiro and Smith, reference 6). A zero-voltage supercurrent is clearly visible. It was not until the experiments of Anderson and Rowe11 (reference 15) that such supercurrents could be definitely ascribed to the tunnelling process.

References: T. Orlando Applied Superconductivity

Macroscopic Quantum Model for Josephson junctions

References: T. Orlando Applied Superconductivity, Chapter 5,8

Reminder: probability current

Schrödinger equation for a single particle (e.g an electron) in a potential $V(\boldsymbol{r})$:

$$i\hbar\frac{\partial\psi}{\partial t} = -\frac{\hbar^2}{2m}\nabla^2\psi + V(\mathbf{r})\psi.$$

According to Born's rule, the square of the magnitude of the wavefunction is interpreted as the probability density of the particle's position:

$$\wp(\mathbf{r},t) \equiv |\psi(\mathbf{r},t)|^2 = \psi^*(\mathbf{r},t)\psi(\mathbf{r},t).$$

This probability density is shown to be conserved by defining a *probability current* f, similar to the continuity equation for the case of charge density and electrical current:

$$\frac{\partial\wp}{\partial t} = -\nabla\cdot\mathbf{J}_\wp,$$

where the *probability current* is defined as

$$\mathbf{J}_\wp \equiv \frac{\hbar}{2im}\left(\psi^*\nabla\psi - \psi\nabla\psi^*\right) = \mathrm{Re}\left\{\psi^*\frac{\hbar}{im}\nabla\psi\right\}.$$

Note: The probability current is not a physical quantity and hence not measurable, in spite of resemblence with the electrical current and the continuity equation.

References: T. Orlando Applied Superconductivity, Chapter 5

Macroscopic Quantum Model for superconductivity

Postulates:

1. Existence of carriers that do not scatter (superelectrons)
2. There exists a macroscopic quantum wavefunction, $\Psi(\mathbf{r},t)$, that describes the behavior of the entire ensemble of super-electrons in the superconductor.

Superconductivity is a coherent phenomenan between all the super-electrons. Similar to the case of coherent state of photons (laser) that describes a global state of a large number of photons.

Single particle:

$$\int dv\psi^*(\mathbf{r},t)\psi(\mathbf{r},t)=1 \rightarrow \begin{cases} \wp(\mathbf{r},t)\equiv\psi^*(\mathbf{r},t)\psi(\mathbf{r},t), & \ldots \text{ probability density} \\ \mathbf{J}_\wp \equiv \mathrm{Re}\left\{\psi^*\frac{h}{im}\nabla\psi\right\}. & \ldots \text{ probability current} \end{cases}$$

Entire ensemble of particles:

$$\int dv\Psi^*(\mathbf{r},t)\Psi(\mathbf{r},t)=\mathbf{N}^* \rightarrow \begin{cases} \Psi^*(\mathbf{r},t)\Psi(\mathbf{r},t)=n^*(\mathbf{r},t), & \ldots \text{ density of particles} \\ \mathbf{J}_\mathrm{s}=\frac{q^\star}{m^*}\,\mathrm{Re}\left\{\Psi^*\frac{\hbar}{i}\nabla\Psi\right\}, & \ldots \begin{array}{l}\text{current of charge} \\ \text{(physical current)}\end{array} \end{cases}$$

where N^* is the number of particles.

References: T. Orlando Applied Superconductivity, Chapter 5

Macroscopic Quantum Model

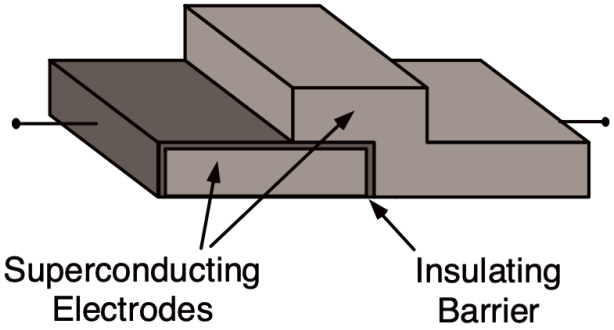

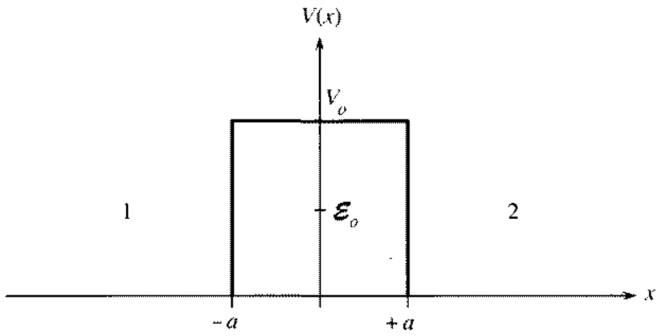

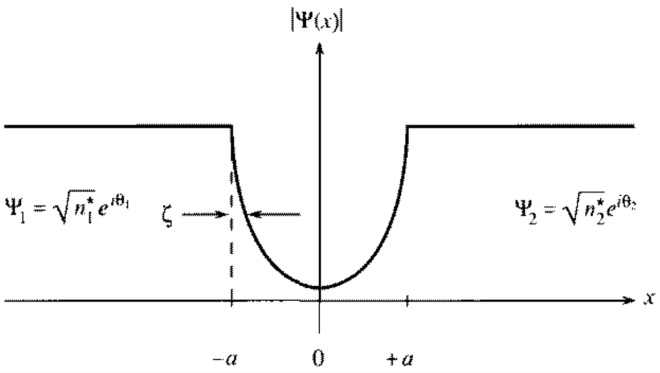

Figure 8.5 The model potential of the insulator $V(x)$ and the magnitude of the wavefunction $|\Psi|$. The two superconductors have densities of superconducting electron pairs $n_1^\star$ and $n_2^\star$, respectively. Furthermore, the phase of the wavefunction θ can be different for the two superconductors at $x = \pm a$.

$$\mathbf{J}_\mathrm{s} = \frac{q^\star}{m^\star} \mathrm{Re}\left\{\Psi^* \frac{\hbar}{i}\nabla\Psi\right\},$$

$$\Psi(+a) = \sqrt{n_2^\star} e^{i\theta_2},$$

$$\Psi(-a) = \sqrt{n_1^\star} e^{i\theta_1},$$

$$\zeta \equiv \sqrt{\frac{\hbar^2}{2m^\star\left(V_o - \mathcal{E}_o\right)}},$$

$$\Psi(x) = C_1 \cosh\frac{x}{\zeta} + C_2 \sinh\frac{x}{\zeta}.$$

References: T. Orlando Applied Superconductivity, Chapter 8

Macroscopic Quantum Model

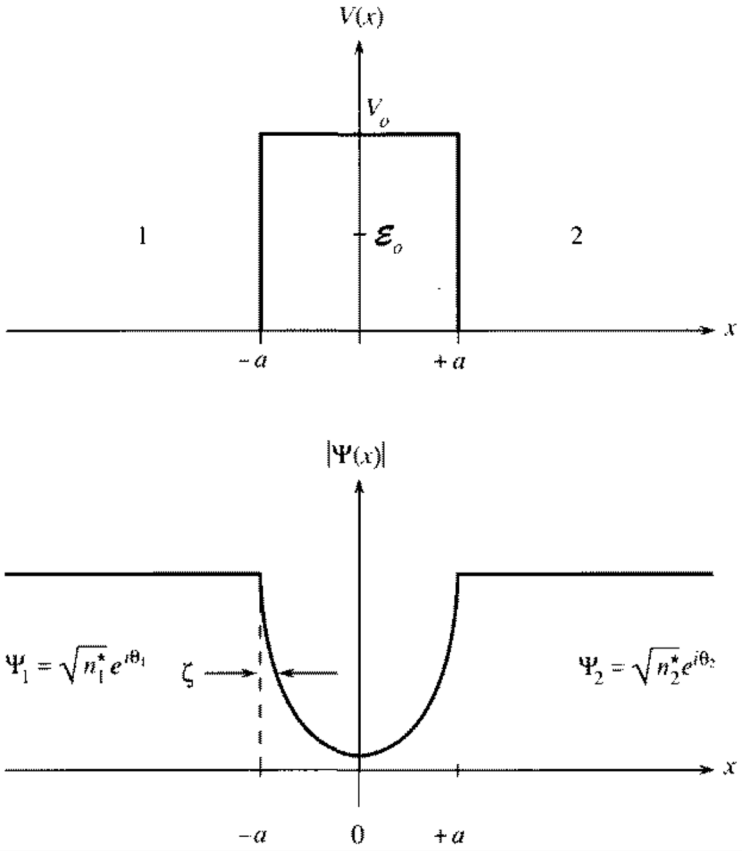

Figure 8.5 The model potential of the insulator $V(x)$ and the magnitude of the wavefunction $|\Psi|$. The two superconductors have densities of superconducting electron pairs $n_1^\star$ and $n_2^\star$, respectively. Furthermore, the phase of the wavefunction θ can be different for the two superconductors at $x = \pm a$.

$$\mathbf{J}_\mathrm{s} = \mathbf{J}_\mathrm{c} \sin\left(\theta_1 - \theta_2\right),$$

$$J_c = -\frac{q^\star \hbar}{m^* \zeta} \frac{\sqrt{n_1^* n_2^*}}{2 \sinh(a/\zeta) \cosh(a/\zeta)} =$$

$$= \frac{e \hbar \sqrt{n_1 n_2}}{2 m \zeta \sinh(2a/\zeta)},$$

$$\sinh 2a/\zeta \approx e^{2a/\zeta}/2.$$

Typical critical current J_C in superconducting qubit: ~ 50 nA (given certain junction area and thickness of insulator layer)

References: T. Orlando Applied Superconductivity

Josephson junctions

$$\mathbf{J}_{\mathrm{s}}(\mathbf{r},t) = \mathbf{J}_{\mathrm{c}}(y,z,t)\sin\varphi(y,z,t),$$

where φ is known as *the gauge-invariant phase difference* and is given by

$$\varphi(y,z,t) = \theta_1(y,z,t) - \theta_2(y,z,t) - \frac{2\pi}{\Phi_o}\int_1^2 \mathbf{A}(\mathbf{r},t)\cdot d\mathbf{l}.$$

$$\frac{\partial\varphi(y,z,t)}{\partial t} = \frac{2\pi}{\Phi_o}\int_1^2 \mathbf{E}(\mathbf{r},t)\cdot d\mathbf{l}$$

The latter equation is known as the Josephson *voltage-phase relation*. Consequently,

$$i = I_c\sin\varphi(t), \quad \frac{d\varphi}{dt} = \frac{2\pi}{\Phi_o}v$$

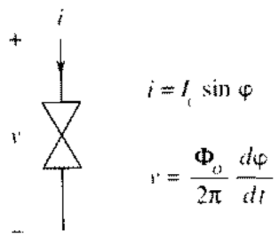

The basic Josephson junction as a lumped circuit parameter is denoted by the crossed symbol in the circuit diagram and is governed by the two equations shown.

References: T. Orlando Applied Superconductivity

Josephson junctions

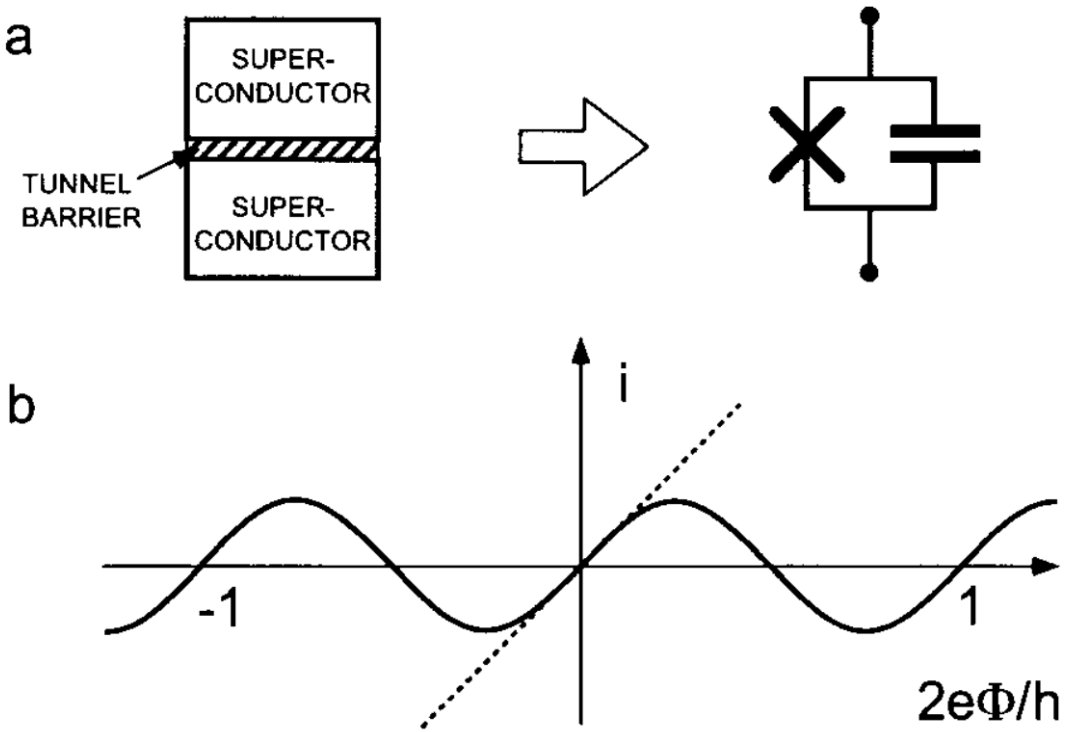

Fig. 2. (a) A Josephson tunnel junction can be modelled as a Josephson tunnel element (cross) in parallel with a capacitor. (b) Current-flux relation of the Josephson element. The dashed line is the current-flux relation of a linear inductance whose value is equal to the effective inductance of the junction.

Relation between phase and flux:

$$\delta = 2\pi\Phi/\Phi_0, \qquad \Phi = \int_{-\infty}^{t} V_J\left(t'\right) dt', \qquad V_J = \frac{\Phi_0}{2\pi}\frac{\mathrm{d}\delta}{\mathrm{d}t}$$

References: Quantum Fluctuations, Les Houches, Devoret 1997

Josephson junctions switching energy

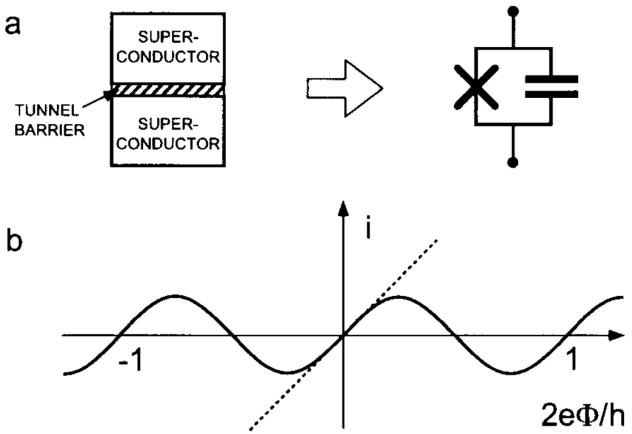

Fig. 2. (a) A Josephson tunnel junction can be modelled as a Josephson tunnel element (cross) in parallel with a capacitor. (b) Current-flux relation of the Josephson element. The dashed line is the current-flux relation of a linear inductance whose value is equal to the effective inductance of the junction.

$$W_J = \int_0^{t_o} ivdt$$

$$W_J = \int_0^{t_o} (I_c \sin\varphi') \left(\frac{\Phi_o}{2\pi} \frac{d\varphi'}{dt} \right) dt$$

$$W_J = \frac{\Phi_o I_c}{2\pi} \int_0^{\varphi} \sin\varphi' d\varphi'$$

$$W_{Jo} = \Phi_o I_c / 2\pi$$

$$W_J = W_{Jo} - \frac{\Phi_o I_c}{2\pi} \cos\varphi$$

Typical value for $W_{J_0} = 2.067 \cdot 10^{-15} \cdot 5 \cdot 10^{-8}/2\pi = 1.65 \cdot 10^{-23}$ J.

References: T. Orlando Applied Superconductivity

The AC Josephson effect

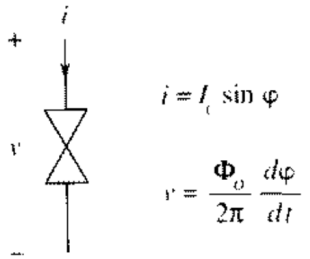

The basic Josephson junction as a lumped circuit parameter is denoted by the crossed symbol in the circuit diagram and is governed by the two equations shown.

$$\varphi(t) = \varphi(0) + \frac{2\pi}{\Phi_o} V_o t$$

$$i = I_c \sin\left[\frac{2\pi}{\Phi_o} V_o t + \varphi(0)\right] = I_c \sin\left[2\pi f_J t + \varphi(0)\right]$$

develops across the junction. This effect is known as the *AC Josephson effect* and f_J is the *Josephson frequency*, given by

$$f_J = \frac{V_o}{\Phi_p} = \frac{2e}{h} V_o = 483.6 \times 10^{12} V_o \text{ (Hz)}.$$

For a constant driving voltage of $10\ \mu\text{V}$, the current will oscillate at about 5 GHz. Because a few microvolts is typical of the lower voltage range applied

References: T. Orlando Applied Superconductivity

Current voltage characteristics of JJ

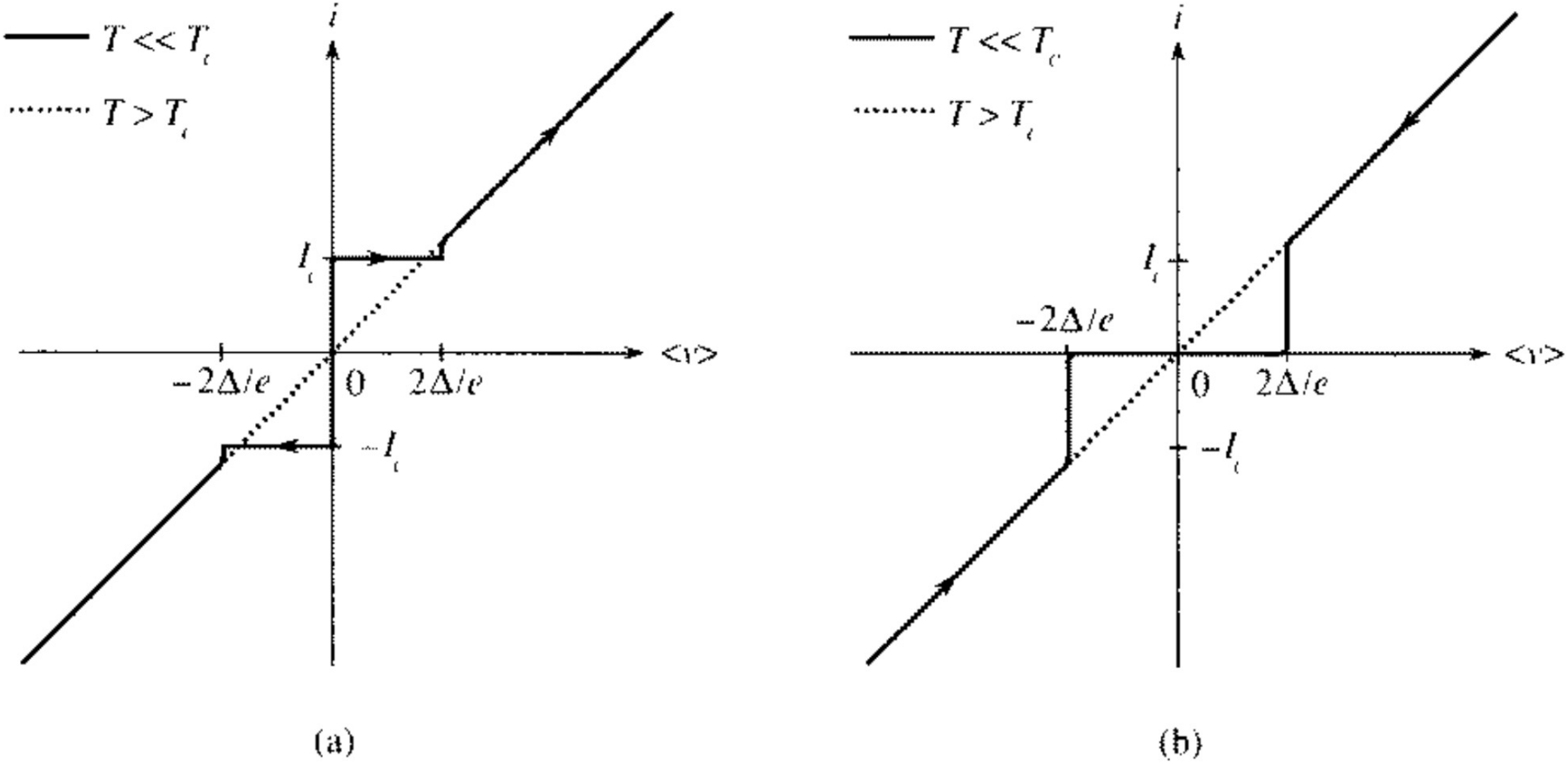

Figure 9.1 Current-voltage characteristic for a constant-current source driving the Josephson junction at a temperature of absolute zero. The voltage is time averaged. Curve (a) is for an increasing driving current and curve (b) is for a decreasing driving current. *Source: Courtesy of D. A. Rudman.*

References: T. Orlando Applied Superconductivity

Generalized Junction model

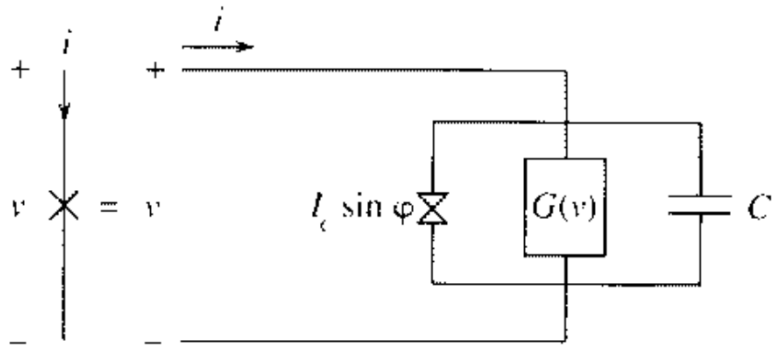

A model of a generalized Josephson junction showing the three parallel channels.

$$i = I_c \sin\varphi + vG(v) + C\frac{dv}{dt}$$

$$i = I_c \sin\varphi + G(v)\frac{\Phi_o}{2\pi}\frac{d\varphi}{dt} + C\frac{\Phi_o}{2\pi}\frac{d^2\varphi}{dt^2}$$

$$i = I_c \sin\varphi + \frac{1}{R}\frac{\Phi_o}{2\pi}\frac{d\varphi}{dt} + C\frac{\Phi_o}{2\pi}\frac{d^2\varphi}{dt^2}$$

$$\frac{i}{I_c} = \sin\varphi + \frac{d\varphi}{d\tilde{\tau}} + \beta_c\frac{d^2\varphi}{d\tilde{\tau}^2}$$

$$\tilde{\tau} = \frac{t}{\tau_J}$$

$$\tau_J = \frac{\Phi_o}{2\pi}\frac{1}{I_c R}$$

References: T. Orlando Applied Superconductivity

Nonlinear Josephson inductance

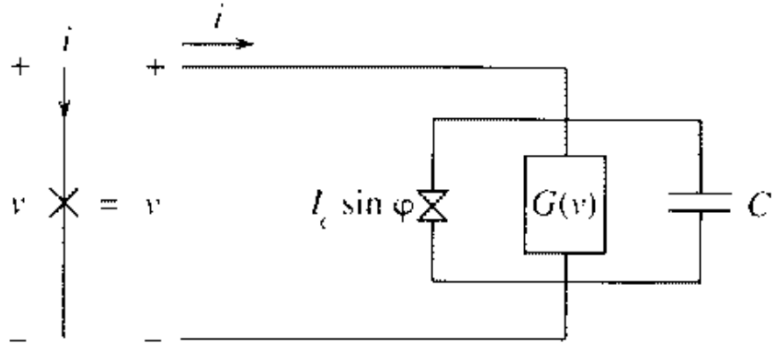

A model of a generalized Josephson junction showing the three parallel channels.

$$i(t) = I_c \sin\varphi(t) + \frac{v(t)}{R},$$

$$\frac{d}{dt} i(t) = \left[\frac{2\pi I_c}{\Phi_o} \cos\varphi(t)\right] v(t) + \frac{1}{R}\frac{d}{dt} v(t).$$

kinetic inductance $L(\varphi)$ and Josephson inductance L_J and are given by

$$L(\varphi) = \frac{\Phi_0}{2\pi I_c \cos\varphi} = \frac{L_J}{\cos\varphi}.$$

References: T. Orlando Applied Superconductivity

SQUID

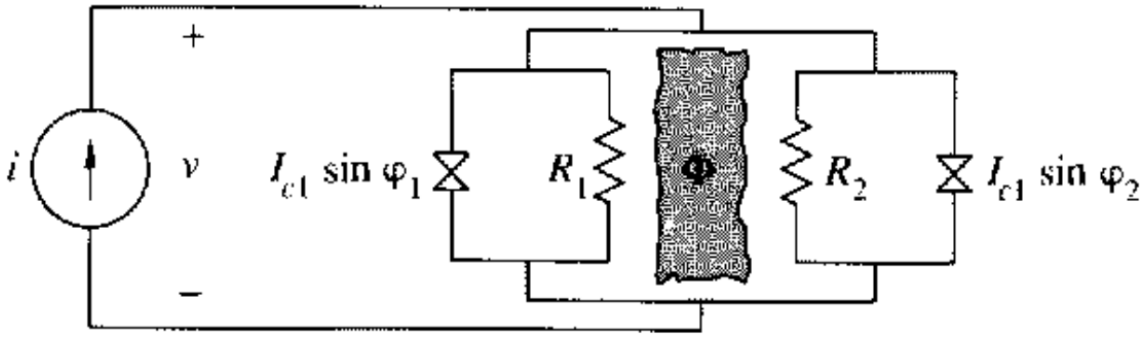

$$\begin{aligned} i &= i_{J_1} + i_{J_2} + i_{R_1} + i_{R_2} \\ &= I_{c1}\sin\varphi_1 + I_{c1}\sin\varphi_2 + \frac{v}{R_1} + \frac{v}{R_2} \end{aligned}$$

$$i = 2I_{c1}\cos\left(\frac{\pi\Phi_{\text{ext}}}{\Phi_o}\right)\sin\left(\varphi_1 + \frac{\pi\Phi_{\text{ext}}}{\Phi_o}\right) + \left(\frac{1}{R_1} + \frac{1}{R_2}\right)v(t)$$

$$I_c = 2I_{c1}\cos\left(\frac{\pi\Phi_{\text{ext}}}{\Phi_o}\right)$$

References: T. Orlando Applied Superconductivity

The Cooper Pair Box

References: Implementation of a superconducting qubit, Cottet, PhD Thesis

Josephson junctions

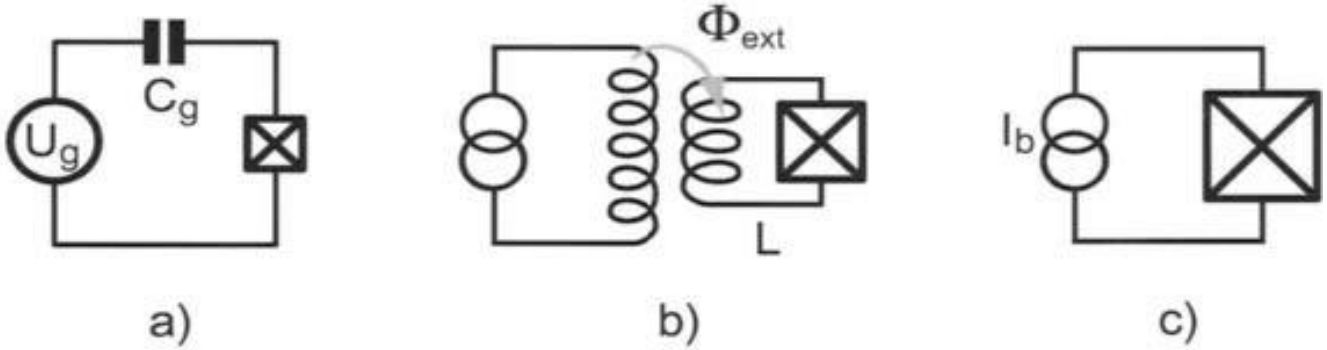

Here $E_C = \frac{(2e)^2}{2(C_J+C_g)}$ is the charging energy of the island of the box and $N_g = Q_r + C_g U/2e$.

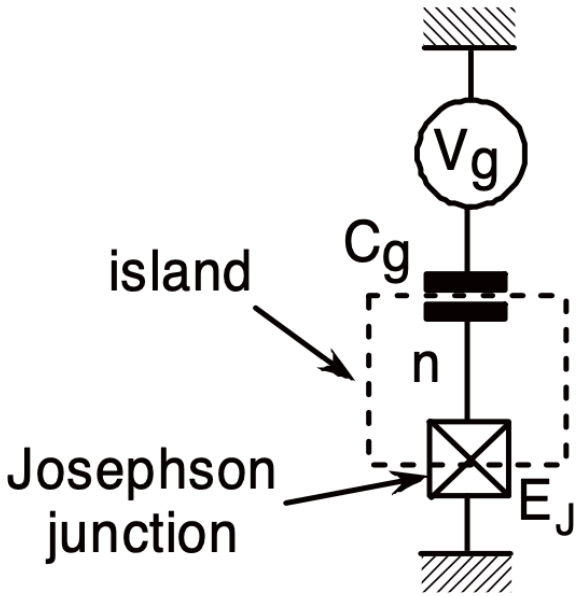

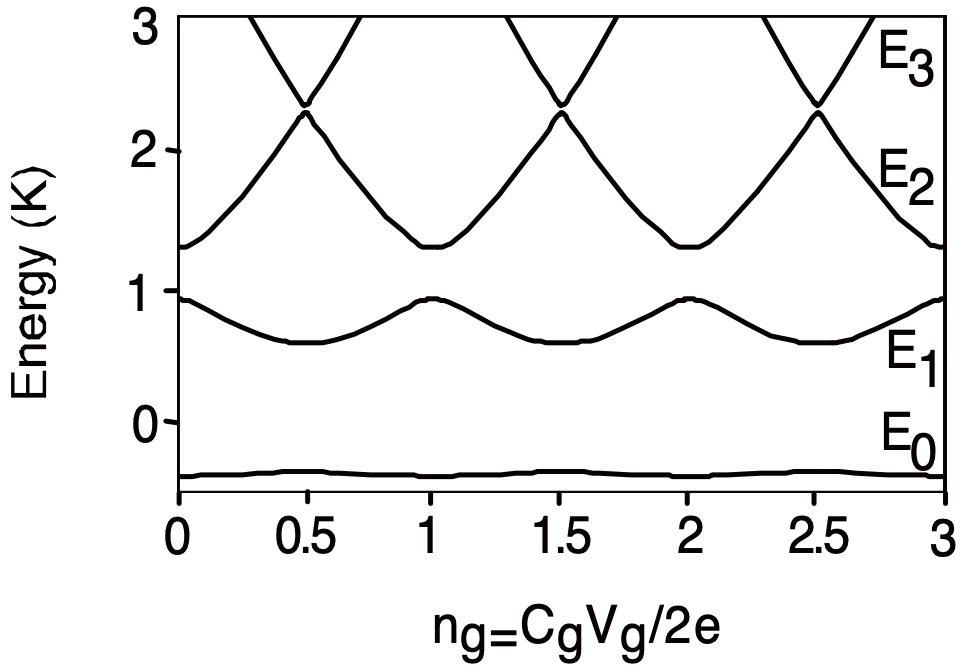

References: Implementation of a superconducting qubit, Cottet, PhD Thesis

Josephson junctions

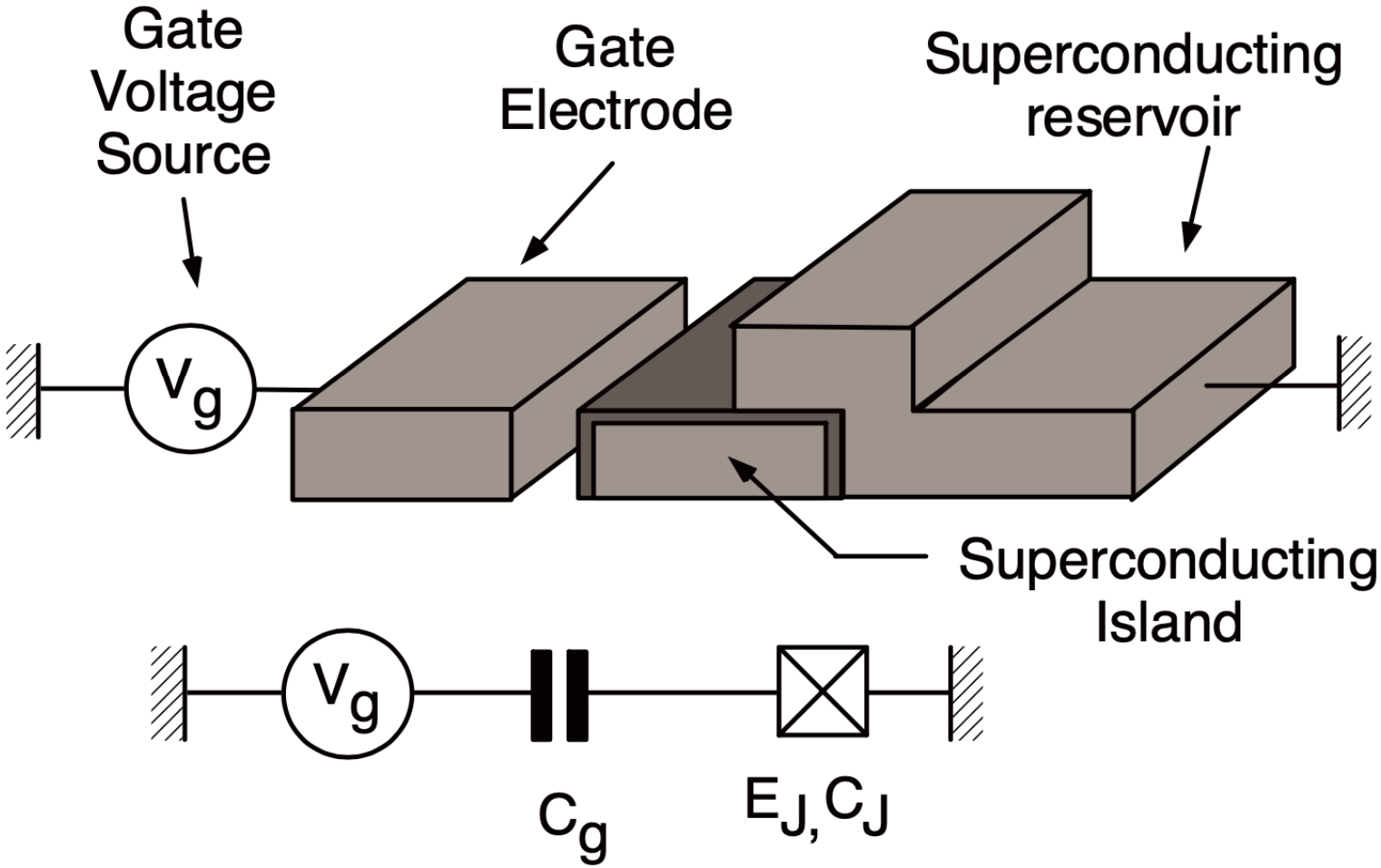

Figure 1.1: *The Cooper pair box. Top: Schematic representation of the Cooper pair box and of its biasing circuit, showing the Josephson junction with energy E_J and capacitance C_J, the superconducting island, the gate, and the gate voltage source V_g. Bottom: Corresponding electrical scheme.*

References: Implementation of a superconducting qubit, Cottet, PhD Thesis

Cooper pair box (CPB)

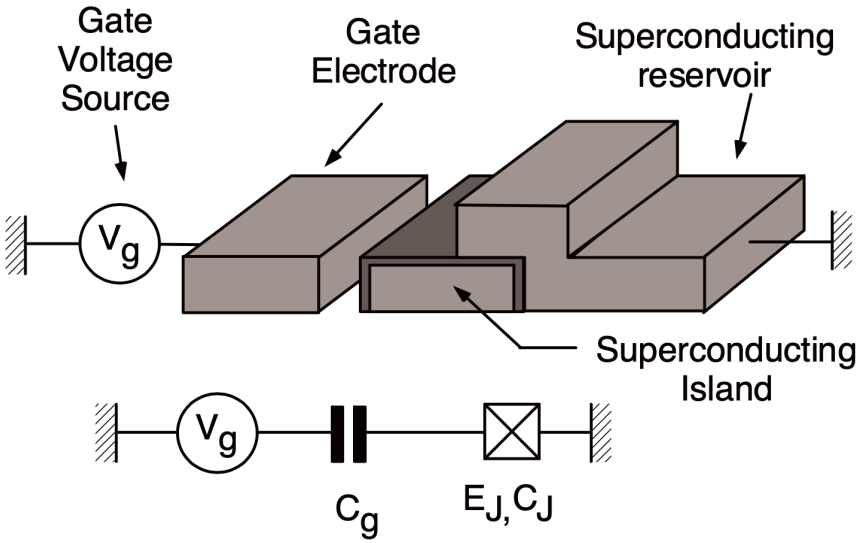

Pair Coulomb energy:

$$E_C = \frac{(2e)^2}{2C_\Sigma},$$

where

$$C_\Sigma = C_g + C_J$$

is the total capacitance of the island[1].

Charge representation

Let $\widehat{\mathbf{n}}$ be the operator associated to the number of Cooper pairs in excess from neutrality in the metallic island (more commonly called "the number of excess Cooper pairs").

The eigenstates $|\mathbf{n}\rangle$ of $\widehat{\mathbf{n}}$ verify:

$$\widehat{H}_{el} = E_C \left(\widehat{\mathbf{n}} - n_g\right)^2,$$

$$n_g = \frac{C_g V_g}{2e}$$

References: Implementation of a superconducting qubit, Cottet, PhD Thesis

[1] We have typically fabricated islands with an area of $1\ \mu\mathrm{m} \times 100\ \mathrm{nm}$ and aluminum Josephson junctions with an area of $100\ \mathrm{nm} \times 100\ \mathrm{nm}$. This results in C_g of the order of $10\ \mathrm{aF}$, C_J of the order of $1\ \mathrm{fF}$, and $E_C \simeq (2e)^2/(2C_J)$ of the order of $4\ \mathrm{k_b K}$. E_J is controlled independently with the oxydation of the junctions and falls in the same range for the experiments we have performed.

Cooper pair box (CPB)

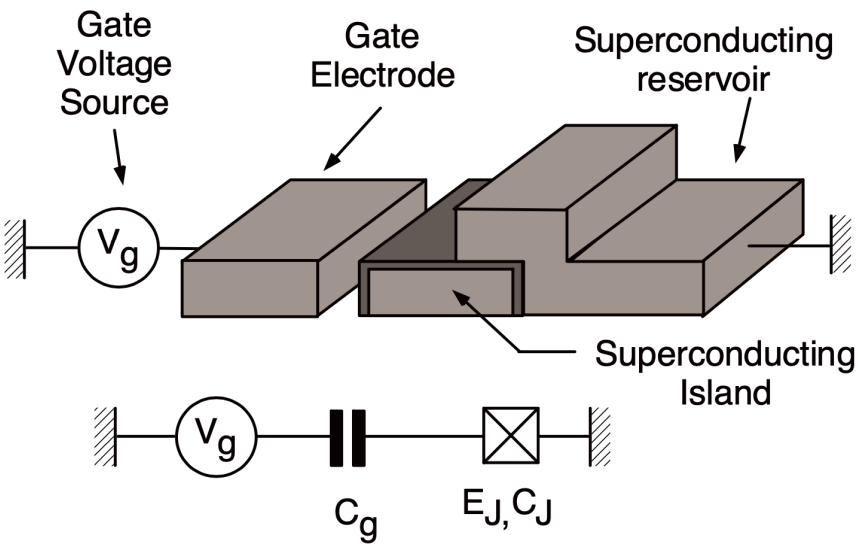

Charge representation

$$\widehat{\mathbf{n}}|\mathbf{n}\rangle = \mathbf{n}|\mathbf{n}\rangle, \mathbf{n} \in \mathbb{Z},$$

$$\widehat{H}_J = -\frac{E_J}{2}\left(\sum_{\mathbf{n}\in\mathbb{Z}} |\mathbf{n}\rangle\langle\mathbf{n}+\mathbf{1}| + |\mathbf{n}+\mathbf{1}\rangle\langle\mathbf{n}|\right),$$

$$\widehat{H}_{el} = E_C\left(\widehat{\mathbf{n}} - n_g\right)^2, \qquad n_g = \frac{C_g V_g}{2e}$$

$$\widehat{H}\left(n_g\right) = \sum_{\mathbf{n}\in\mathbb{Z}}\left[E_C\left(\mathbf{n}-n_g\right)^2|\mathbf{n}\rangle\langle\mathbf{n}| - \frac{E_J}{2}\left(|\mathbf{n}\rangle\langle\mathbf{n}+\mathbf{1}| + |\mathbf{n}+\mathbf{1}\rangle\langle\mathbf{n}|\right)\right]$$

The spectrum associated to this hamiltonian is discrete and periodic in n_g. Let us call $|k\rangle$ the energy eigenstates and E_k their associated energies:

$$\widehat{H}\left(n_g\right)|k\rangle = E_k|k\rangle.$$

References: Implementation of a superconducting qubit, Cottet, PhD Thesis

Cooper pair box (CPB)

$$\widehat{H}\left(n_g\right) = \sum_{\mathbf{n}\in\mathbb{Z}} \left[E_C \left(\mathbf{n} - n_g\right)^2 |\mathbf{n}\rangle\langle\mathbf{n}| - \frac{E_J}{2}\left(|\mathbf{n}\rangle\langle\mathbf{n+1}| + |\mathbf{n+1}\rangle\langle\mathbf{n}|\right)\right]$$

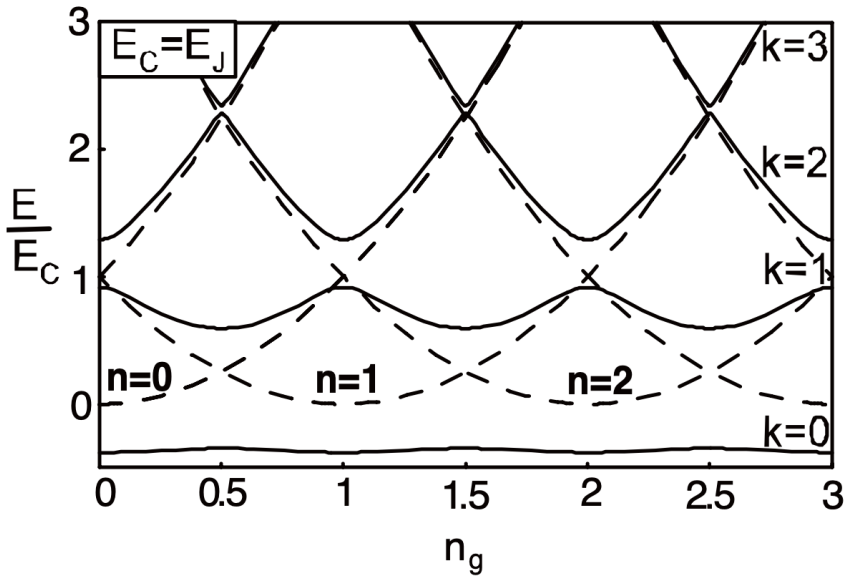

Figure 1.2: *Full lines: Eigenenergies of a Cooper pair box with $E_C = E_J$, calculated by diagonalizing the hamiltonian $\widehat{H}$ in the charge representation, in a subspace of 10 charge states. Dotted lines: Electrostatic energies of the charge states. Note that the degeneracies between the energies of neighbouring charge states occurring at $n_g = \frac{1}{2}$ [mod 1] are lifted by the Josephson coupling.*

References: Implementation of a superconducting qubit, Cottet, PhD Thesis

Cooper pair box (CPB)

Phase representation

Conjugate of a 2e-quantized charge

According to the BCS theory, the conjugate of the number $\widehat{N}$ of Cooper pairs in an electrode is the superconducting phase $\widehat{\theta}$ of the electrode. The conjugate of the number $\widehat{N}$ of Cooper pairs having passed through a Josephson junction, is the superconducting phase difference $\widehat{\theta}$ through the junction. Let us note $|\theta\rangle$ the eigenstates of $\widehat{\theta}$:

$$\widehat{\theta}\,|\theta\rangle = \theta\,|\theta\rangle \ ,$$

with $\theta \in \mathbb{R}$. In the BCS theory, the discreteness of $\widehat{N}$ causes that $|\theta\rangle$ and $|\theta + 2\pi\rangle$ have the same physical meaning. As a consequence, in order to describe the states of the node or branch, it is enough to work on the basis $\{|\theta\rangle\,, \theta \in [0, 2\pi[\}$.

Quantized charge case

In the case of a quantized number of charge $\widehat{\mathbf{n}}$, the relations (1.82) must include the charge $\widehat{Q} = 2e\widehat{\mathbf{n}}$. The relationship between the superconducting phase $\widehat{\theta}$ conjugated to $\widehat{\mathbf{n}}$ and the flux $\widehat{\Phi}$ included in the Equations (1.83) and (1.84) is:

$$\widehat{\theta} = \widehat{\Phi}/\varphi_0 \ [\mathrm{mod}\ \ 2\pi] \ . \tag{1.85}$$

References: Implementation of a superconducting qubit, Cottet, PhD Thesis (Chapter 1)

Quantum fluctuations in Josephson junction

The superconducting tunnel junction can be modeled by a capacitor in parallel with a pure tunneling element, the Josephson junction. The Cooper pairs that tunnel through the junction can be expressed in the **charge basis**

$$Q_J(t) = -2eN(t), \quad \widehat{N} = \sum_N N|N\rangle\langle N|.$$

Josephson junction **Phase operator**

$$|\delta\rangle = \sum_{N=-\infty}^{+\infty} \mathrm{e}^{iN\delta}|N\rangle, \quad |N\rangle = \frac{1}{2\pi}\int_0^{2\pi} d\delta \mathrm{e}^{-iN\delta}|\delta\rangle, \quad [\widehat{\delta}, \widehat{N}] = i$$

Introducing the operator:

$$\mathrm{e}^{i\hat{\delta}} = \frac{1}{2\pi}\int_0^{2\pi} d\delta \mathrm{e}^{i\delta}|\delta\rangle\langle\delta|$$

Yields:

$$\mathrm{e}^{i\widehat{\delta}}|N\rangle = |N-1\rangle$$

Note, in contrast to quantum optics, where no phase operator can be defined, phase and n umber operator are here canonically conjugate operators as N can be negative.

$$\begin{aligned}
e^{i\phi}|N\rangle &= \frac{1}{2\pi}\int_0^{2\pi} \mathrm{d}\phi e^{i\phi}|\phi\rangle\langle\phi|N\rangle \\
&= \frac{1}{2\pi}\int_0^{2\pi} \mathrm{d}\phi e^{i\phi}|\phi\rangle \sum_M e^{-iM\phi}\langle M|N\rangle \\
&= \frac{1}{2\pi}\int_0^{2\pi} \mathrm{d}\phi e^{i\phi}|\phi\rangle \sum_M e^{-iM\phi\delta_{MN}} \\
&= \frac{1}{2\pi}\int_0^{2\pi} \mathrm{d}\phi e^{i\phi}\mathrm{e}^{-iN\phi}|\phi\rangle \\
&= \frac{1}{2\pi}\int_0^{2\pi} \mathrm{d}\phi e^{-i(N-1)\phi}|\phi\rangle = |\mathrm{N}-1\rangle
\end{aligned}$$

References: Les Houches 1997 Quantum Fluctuations, Devoret

Hamiltonian description of the J-Junction

Hamiltonian of the Josephson tunnel Junction using the phase operator

$$\widehat{h}_J = -E_J \cos\widehat{\delta}, \qquad E_J = \frac{1}{8}\frac{h}{e^2} G_t \Delta,$$

where Δ is the superconducting gap and G_t the tunnel conductance in the normal.

Re-expressing the Hamiltonian in the charge Basis of cooper pairs (N) that tunnel through the junction.

$$\widehat{h}_J = -\frac{E_J}{2}\frac{1}{2\pi}\int_0^{2\pi} d\delta \left[\mathrm{e}^{i\delta} + \mathrm{e}^{-i\delta}\right] |\delta\rangle\langle\delta|,$$

$$\mathrm{e}^{i\widehat{\delta}}|N\rangle = |N-1\rangle, \quad \mathrm{e}^{i\widehat{\delta}} = \frac{1}{2\pi}\int_0^{2\pi} d\delta \mathrm{e}^{i\delta}|\delta\rangle\langle\delta|,$$

$$\widehat{h}_J = -\frac{E_J}{2}\sum_{N=-\infty}^{+\infty} [|N\rangle\langle N+1| + |N+1\rangle\langle N|].$$

References: Les Houches 1997 Quantum Fluctuations, Devoret

The phase representation

Properties of conjugate variables

Because of the circular topology of the phase space associated to $\widehat{\theta}$, physical expressions can only contain $\widehat{\theta}$ through trigonometric expressions. The analog of formulas (1.72) are the Fourier transforms between the eigenstates $\{|\mathbf{n}\rangle, \mathbf{n} \in \mathbb{Z}\}$ of $\widehat{\mathbf{n}}$ and the eigenstates $\{|\theta\rangle, \theta \in [0, 2\pi[\}$ of $\widehat{\theta}$ [51]:

$$|\theta\rangle = \frac{1}{\sqrt{2\pi}} \sum_{\mathbf{n}\in\mathbb{Z}} \exp(\mathbf{i}\widehat{\mathbf{n}}\theta) |\mathbf{n}\rangle \Leftrightarrow |\mathbf{n}\rangle = \frac{1}{\sqrt{2\pi}} \int_0^{2\pi} d\theta \exp(-\mathbf{i}\widehat{\mathbf{n}}\theta) |\theta\rangle \ . \tag{1.74}$$

This relation ensures the validity of some fundamental properties likes the translational relations:

$$\exp(\mathbf{i}p\widehat{\theta}) |\mathbf{n}\rangle = |\mathbf{n}+p\rangle \tag{1.75}$$

and

$$\exp(-\mathbf{i}\theta_0\widehat{\mathbf{n}}) |\theta\rangle = |\theta - \theta_0\rangle \ , \tag{1.76}$$

with $\mathbf{p} \in \mathbb{N}$ and $\theta_0 \in \mathbb{R}$. It also infers that $\widehat{\mathbf{n}}$ can be expressed in the phase space as:

$$\widehat{\mathbf{n}} = \frac{1}{\mathbf{i}} \frac{\partial}{\partial\theta} \ , \tag{1.77}$$

and that $\widehat{\theta}$ can be expressed in the charge space as:

$$\widehat{\theta} = \mathbf{i} \frac{\partial}{\partial\mathbf{n}} \ . \tag{1.78}$$

Eventually, for any observable $\widehat{A}$,

$$\left[\widehat{A}, \widehat{H}\right] = \mathbf{i}\hbar \frac{\partial \widehat{A}}{\partial t} \ , \tag{1.79}$$

$$\left[\widehat{A}, \widehat{\mathbf{n}}\right] = \mathbf{i} \frac{\partial \widehat{A}}{\partial \widehat{\theta}} \ , \tag{1.80}$$

and:

$$\left[\widehat{A}, \widehat{\theta}\right] = -\mathbf{i} \frac{\partial \widehat{A}}{\partial \widehat{\mathbf{n}}} \ . \tag{1.81}$$

References: Implementation of a superconducting qubit, Cottet, PhD Thesis (Chapter 1)

Contrast with phase operator in quantum Optics

For a harmonic oscillator (in particular the electromagnetic field) with the Hamiltonian $\widehat{H} = \hbar\omega\left(\widehat{a}^{\dagger}\hat{a} + \frac{1}{2}\right)$, it is possible to define a "phase operator" in analogy with the classical case:

$$\hat{a} = e^{i\hat{\phi}}\sqrt{\hat{n}},$$
$$\hat{a}^{\dagger} = \sqrt{\hat{n}}e^{-i\hat{\phi}},$$

with $\hat{n} = \hat{a}^{\dagger}\hat{a}$ and $\hat{\phi}$ being the hypothetical Hermitian phase operator.

This operator satisfies many identities similar to the previously defined superconducting phase operator $\hat{\theta}$, namely $[\hat{n}, \hat{\theta}] = i$, But careful calculation reveals that it is in fact not a well defined Hermitian operator. For example it is easy to show the commutator $[e^{i\hat{\phi}}, e^{-i\hat{\phi}}]$ is not equal to zero (see the exercise), which is a sign of inconsistency. This inconsistency in fact arises dew to fact that the Hilbert space for the harmonic oscillator is given by $n \in \mathbb{N}$. In the case of the superconducting phase the Hilbert space of the Cooper pares also extends to negative values, allowing the well defined phase operator.

References: [1] P. A. M. Dirac, The Quantum Theory of the Emission and Absorption of Radiation, Proc. R. Soc. Lond., A 114 (1927), 243. [2] Quantum Optics, D.F. Walls, Gerard J. Milburn Chapter (2)

Cooper pair box (CPB)

Phase representation

$$\widehat{\theta}|\theta\rangle = \theta|\theta\rangle \qquad |\theta\rangle \equiv |\theta + 2\pi\rangle$$

$$\exp\left(\pm\mathbf{i}\widehat{\theta}\right)|\mathbf{n}\rangle = |\mathbf{n} \pm 1\rangle \qquad \widehat{\mathbf{n}} = \frac{1}{\mathbf{i}}\frac{\partial}{\partial\theta}$$

Hamiltonian in the phase representation

$$H\left(n_g\right) = E_C\left(\frac{1}{\mathbf{i}}\frac{\partial}{\partial\theta} - n_g\right)^2 - E_J\cos(\theta)$$

$$\Psi_k(\theta) = \langle\theta|k\rangle$$

$$E_C\left(\frac{1}{\mathbf{i}}\frac{\partial}{\partial\theta} - n_g\right)^2\Psi_k(\theta) - E_J\cos(\theta)\Psi_k(\theta) = E_k\Psi_k(\theta)$$

$$\Psi_k(\theta) = \Psi_k(\theta + 2\pi)$$

References: Implementation of a superconducting qubit, Cottet, PhD Thesis (Chapter 1)

Cooper pair box (CPB)

the function

$$\varphi_k(\theta) = \exp(-\mathbf{i}n_g\theta)\Psi_k(\theta)$$

is a solution of the equation:

$$-E_C\frac{\partial^2}{\partial\theta^2}\varphi_k(\theta) - E_J\cos(\theta)\varphi_k(\theta) = E_k\varphi_k(\theta)\ . \tag{1.18}$$

The equation (1.18) takes the form of a Mathieu equation:

$$\frac{\partial^2 y(z)}{\partial z^2} - 2q\cos(2z)y(z) = -ay(z)\ ,\ z\in\ ]-\infty,+\infty[\ , \tag{1.19}$$

with

$$\theta = 2z,\ \ y(z) = \varphi_k(2z),\ \ q = -2E_J/E_C,\ \ a = 4E_k/E_C\ . \tag{1.20}$$

The solutions of this equation are analytically known [44]. The Mathieu functions[3] $\mathcal{M}_C(a,q,z)$ and $\mathcal{M}_S(a,q,z)$, are the textbook solutions of (1.19) respectively even and odd in z . Note that when $q = 0$, these Mathieu functions are simply:

$$\begin{aligned}\mathcal{M}_C(a,0,z) &= \cos(\sqrt{a}z)\\ \mathcal{M}_S(a,0,z) &= \sin(\sqrt{a}z)\ .\end{aligned} \tag{1.21}$$

References: Implementation of a superconducting qubit, Cottet, PhD Thesis (Chapter 1)

Cooper pair box (CPB)

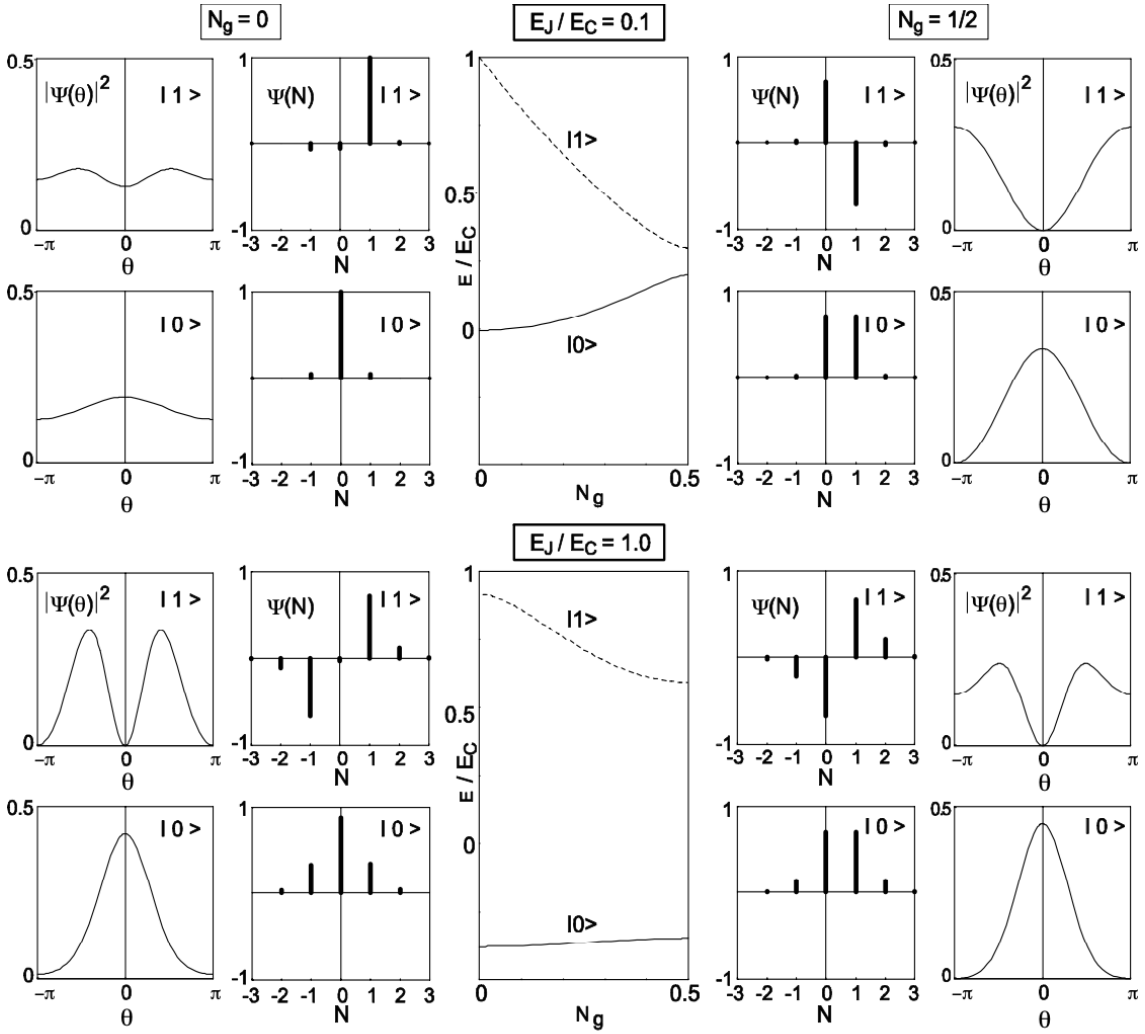

Fig. 3. Eigenenergies (middle panels) and wavefunctions of the $|0\rangle$ and $|1\rangle$ states in the charge and phase representations, for $N_g = 0$ (left panels) and for $N_g = 1/2$ (right panels), and for E_J/E_C ratios equal to 0.1 (top panels) and 1 (bottom panels). The $\Psi_k(N)$ eigenvectors are directly represented since they can be chosen real, whereas the $\Psi_k(\theta)$ wavefunctions are represented by their modulus squared.

References: JOSEPHSON QUANTUM BITS BASED ON A COOPER PAIR BOX, Denis Vion

Josephson junctions

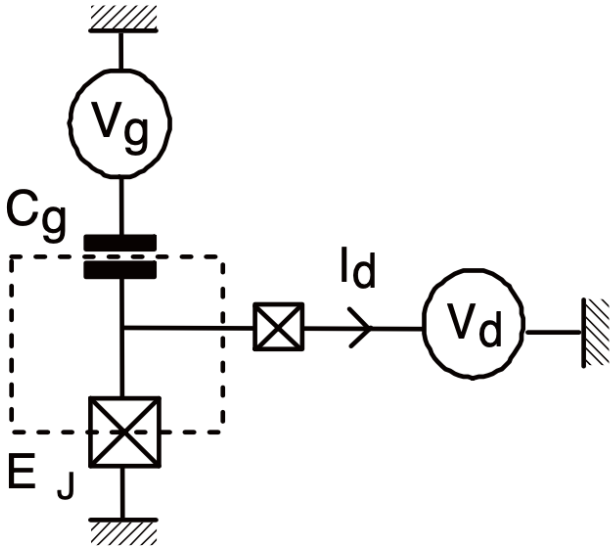

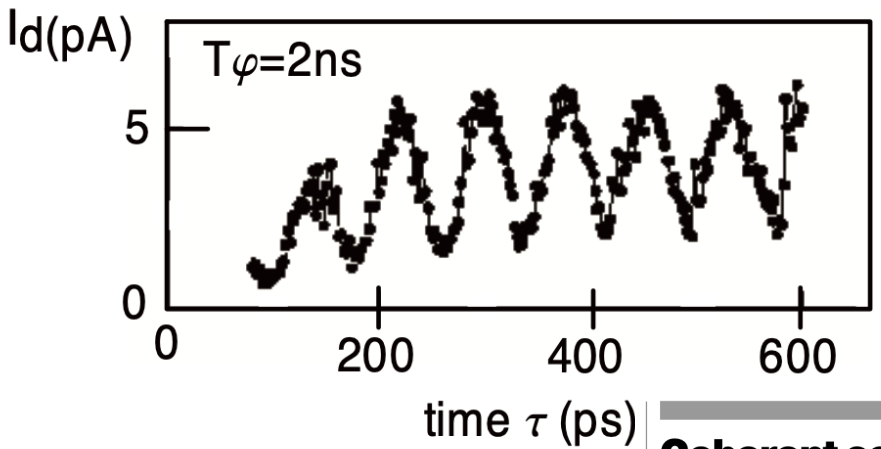

Coherent control of macroscopic quantum states in a single-Cooper-pair box

Y. Nakamura*, Yu. A. Pashkin† & J. S. Tsai*

** NEC Fundamental Research Laboratories, Tsukuba, Ibaraki 305-8051, Japan*
† CREST, Japan Science and Technology Corporation (JST), Kawaguchi, Saitama 332-0012, Japan

Figure 4: *Coherent manipulation of the quantum state of a Cooper pair box, in the experiment of Y. Nakamura et al.* [19]. *Left panel: Simplified electrical scheme of the experiment. A fast voltage pulse is applied to the gate to bring the system at the charge degeneracy point* $n_g = 1/2$. *The sudden change of the hamiltonian induces Rabi oscillations between the* $|0\rangle$ *and* $|1\rangle$ *states during the pulse duration* τ. *Right panel: Oscillations of the occupation probability of state* $|1\rangle$ *are revealed by oscillations of the current probe* I_d *with* τ.

References: Nakamura Science

Josephson junctions

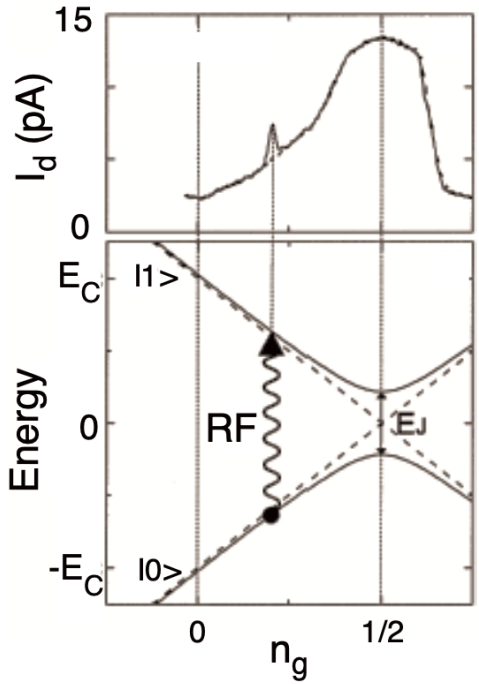

Figure 5: *Spectroscopy of the Cooper pair box. The energy difference between states* $|0\rangle$ *and* $|1\rangle$ *is measured by applying to the gate continuous radiofrequency signals at different frequencies and by sweeping the gate charge* n_g*. Top panel: A resonant increase of the current* I_d *through the probe junction (see text) is observed when* n_g *is such that the energy difference matches the applied frequency. Bottom panel: Energy diagram illustrating the excitation of the box by radiofrequency irradiation. Solid lines represent eigenenergies of the box whereas dashed lines show the electrostatic energy of charge states.*

References: Implementation of a superconducting qubit, Cottet, PhD Thesis

Manipulating the Quantum State of an Electrical Circuit

D. Vion,* A. Aassime, A. Cottet, P. Joyez, H. Pothier, C. Urbina,† D. Esteve, M. H. Devoret‡

We have designed and operated a superconducting tunnel junction circuit that behaves as a two-level atom: the "quantronium." An arbitrary evolution of its quantum state can be programmed with a series of microwave pulses, and a projective measurement of the state can be performed by a pulsed readout subcircuit. The measured quality factor of quantum coherence $Q_\varphi \cong 25{,}000$ is sufficiently high that a solid-state quantum processor based on this type of circuit can be envisioned.

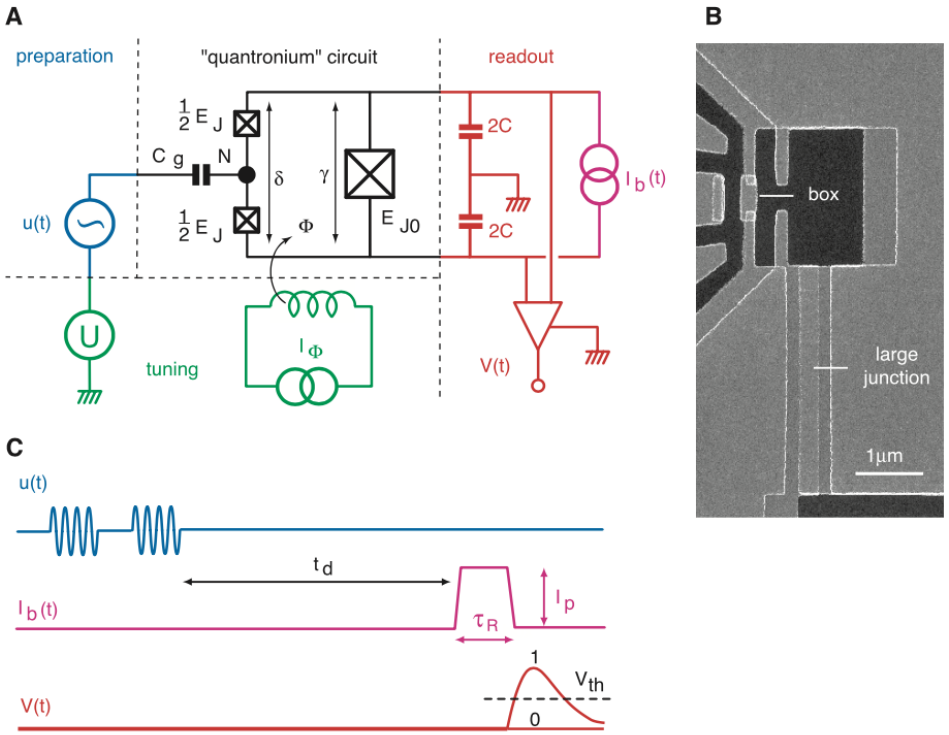

Fig. 1. (**A**) Idealized circuit diagram of the quantronium, a quantum-coherent circuit with its tuning, preparation, and readout blocks. The circuit consists of a Cooper pair box island (black node) delimited by two small Josephson junctions (crossed boxes) in a superconducting loop. The loop also includes a third, much larger Josephson junction shunted by a capacitance C. The Josephson energies of the box and the large junction are E_J and E_{J0}. The Cooper pair number N and the phases δ and γ are the degrees of freedom of the circuit. A dc voltage U applied to the gate capacitance C_g and a dc current I_Φ applied to a coil producing a flux Φ in the circuit loop tune the quantum energy levels. Microwave pulses $u(t)$ applied to the gate prepare arbitrary quantum states of the circuit. The states are read out by applying a current pulse $I_b(t)$ to the large junction and by monitoring the voltage $V(t)$ across it. (**B**) Scanning electron micrograph of a sample. (**C**) Signals involved in quantum state manipulation and measurement. Top: Microwave voltage pulses $u(t)$ are applied to the gate for state manipulation. Middle: A readout current pulse $I_b(t)$ with amplitude I_p is applied to the large junction t_d after the last microwave pulse. Bottom: Voltage $V(t)$ across the junction. The occurrence of a pulse depends on the occupation probabilities of the energy eigenstates. A discriminator with threshold V_{th} converts $V(t)$ into a boolean output for statistical analysis.

References: D. Vion, et al. Science

The transmon qubit

Transmon: a transmission-line shunted plasma oscillation qubit

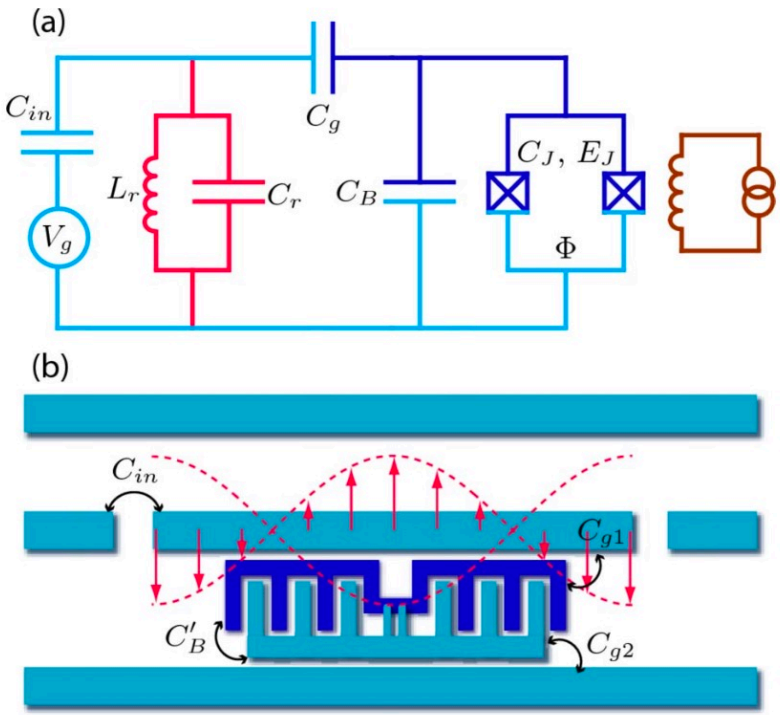

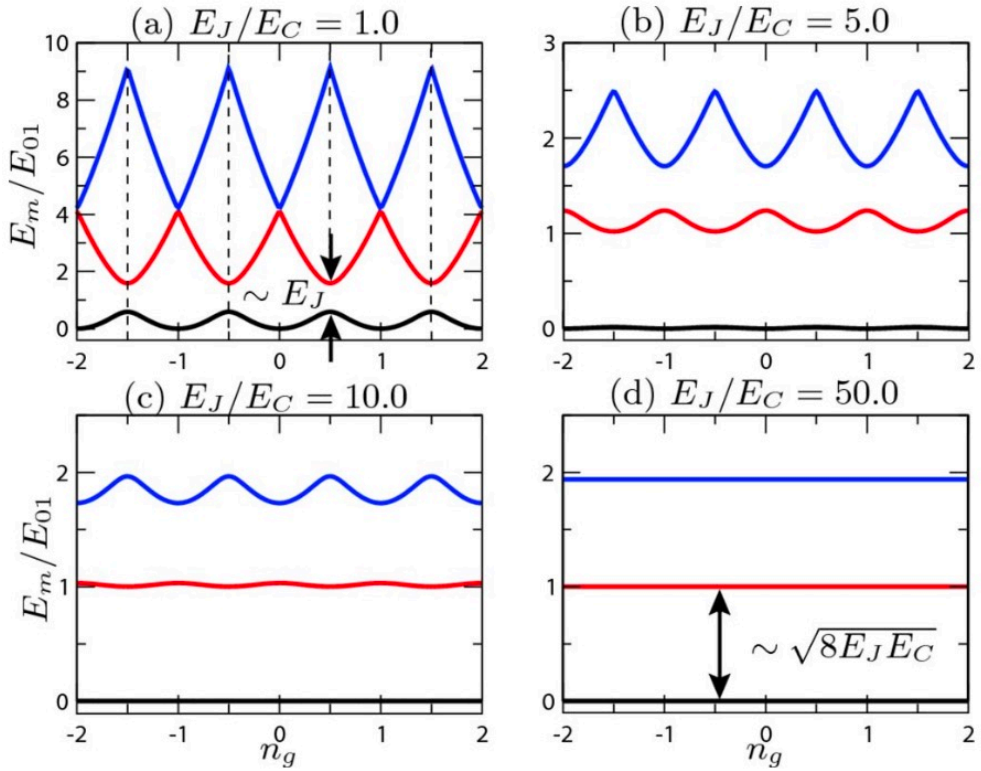

1. Large ratio of Josephson energy to charge energy E_J/E_C
2. More insensitive to charge noise
3. Longer dephasing times

References: Physical Review A, 76,042319

Circuit Quantization and anharmonicity

Hamiltonian of transmon qubit:

$$H = 4E_C n^2 - E_J \cos\delta, \quad \cos\delta \approx 1 - \frac{\delta^2}{2!} + \frac{\delta^4}{4!} + \cdots$$

To lowest order, we have the harmonic oscillator Hamiltonian:

$$H \approx 4E_C n^2 + E_J \frac{\delta^2}{2} = \sqrt{8E_J E_C}\left(a^\dagger a + \frac{1}{2}\right)$$

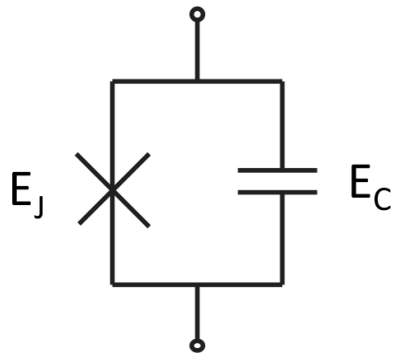

Where n, δ is the conjugate pair of position and momentum:

$$\delta = \left(\frac{2E_C}{E_J}\right)^{1/4}\left(a + a^\dagger\right),$$

$$n = -i\left(\frac{E_J}{8E_C}\right)^{1/4}\frac{1}{\sqrt{2}}\left(a - a^\dagger\right).$$

So the Hamiltonian keeping up to the fourth order of δ is:

$$H \approx 4E_C n^2 + \frac{E_J\delta^2}{2} - \frac{\delta^4}{24} = \sqrt{8E_J E_C}\left(a^\dagger a + \frac{1}{2}\right) - \frac{E_C}{12E_J}\left(a + a^\dagger\right)^4$$

References: Physical Review A, 76,042319

Circuit Quantization and anharmonicity

Correct the quartic term for each energy level:

$$\begin{aligned}\Delta E_m &= \langle m| - E_J \frac{\delta^4}{24} |m\rangle \\ &= -\frac{E_C}{12} \langle m| \left(a + a^\dagger\right)^4 |m\rangle \\ &= -\frac{E_C}{12} \left(6m^2 + 6m + 3\right).\end{aligned}$$

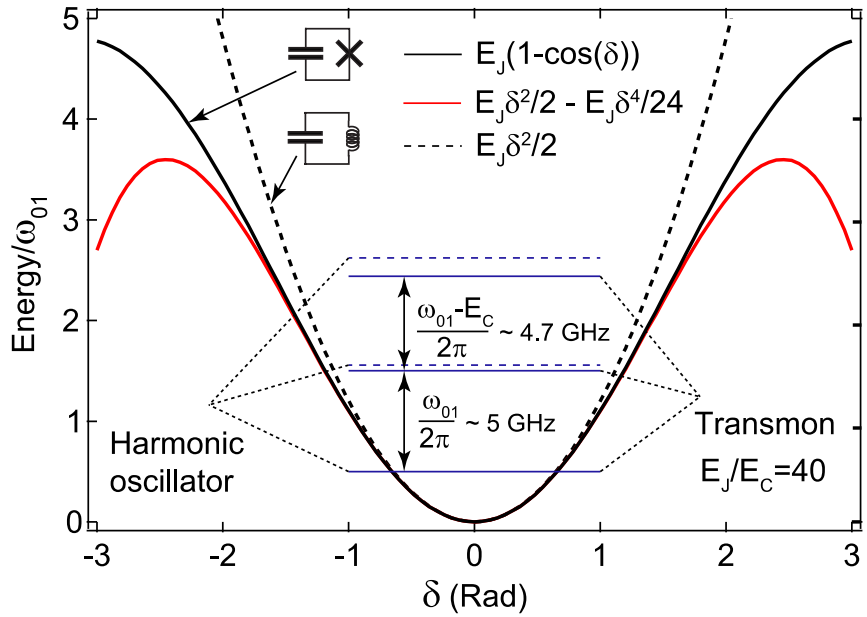

Corrected energy level for transmon qubit:

$$E_m = m\sqrt{8E_J E_C} - \frac{E_C}{12}\left(6m^2 + 6m + 3\right).$$

Lowest energy of transmon qubit,

$$E_{10} = E_1 - E_0 = \sqrt{8E_J E_C} - E_C,$$

Anharmonicity:

$$\eta = \omega_{21} - \omega_{10} = \left(E_{21} - E_{10}\right)/\hbar = -E_C/\hbar.$$

The relative anharmonicity $\eta_r \equiv \frac{\eta}{E_{10}} \approx -\left(\frac{8E_J}{E_C}\right)^{-\frac{1}{2}}$ decrease algebraically with E_J/E_C.

Charge dispersion decrease exponentially with E_J/E_C: (in large E_J/E_C approximation)

$E_m\left(n_g\right) \simeq E_m\left(n_g = 1/4\right) - \frac{\epsilon_m}{2}\cos\left(2\pi n_g\right)$,
where $\epsilon_m \equiv E_m\left(n_g = 1/2\right) - E_m\left(n_g = 0\right)$

$$\epsilon_m \simeq (-1)^m E_C \frac{2^{4m+5}}{m!}\sqrt{\frac{2}{\pi}}\left(\frac{E_J}{2E_C}\right)^{\frac{m}{2}+\frac{3}{4}} e^{-\sqrt{8E_J/E_C}},$$

Exploiting these facts, transmon qubit operates on $\frac{E_J}{E_C} \gg 1$ (transmon regime).

References: Exploring Quantum Dynamics and Thermodynamics in Superconducting Qubit, M. Naghiloo, PhD Thesis

Josephson junctions

In the absence of junction nonlinearity, one can solve the normal modes of the electrical circuit:

$$\sum_m \hbar\omega_m \hat{a}_m^\dagger \hat{a}_m.$$

Introducing the Bosonic operators for the Josephson phase:

$$\hat{\varphi}_{m,j} = \varphi_{\mathrm{zpf},m,j}\left(\hat{a}_m + \hat{a}_m^\dagger\right),$$

$$\varphi_{\mathrm{zpf},m,j} = \frac{1}{\phi_0}\sqrt{\frac{\hbar}{2\omega_m C_m}}.$$

Introducing the Bosonic operators for the Josephson phase, and Taylor expanding leads to the expression (note that the quadratic part of the cosine potential gives rise to the normal modes and is therefore removed from the expansion below).

$$\hat{H} = \sum_m \hbar\omega_m \hat{a}_m^\dagger \hat{a}_m + \sum_j \sum_{n\geq 2} E_j \frac{(-1)^{n+1}}{(2n)!}\hat{\varphi}_j^{2n},$$

$$\hat{H} = \sum_m \hbar\omega_m \hat{a}_m^\dagger \hat{a}_m + E_j\left[1 - \cos\hat{\varphi}_j - \frac{\hat{\varphi}_j^2}{2}\right].$$

Paper for this week

Strong coupling of a single photon to a superconducting qubit using circuit quantum electrodynamics

A. Wallraff[1], D. I. Schuster[1], A. Blais[1], L. Frunzio[1], R.- S. Huang[1,2], J. Majer[1], S. Kumar[1], S. M. Girvin[1] & R. J. Schoelkopf[1]

[1]*Departments of Applied Physics and Physics, Yale University, New Haven, Connecticut 06520, USA*
[2]*Department of Physics, Indiana University, Bloomington, Indiana 47405, USA*

Paper for this week

- What is the Jaynes-Cummings (JC) model between a two-level system and quantized photons, what the difference to the semi-classical atom-light interaction
- How does the physical system map to the JC model (what are the "atom" and "photon cavity")
- How do they tune the frequency of the "atom" to match that of the "cavity". How's the measured response changing?
- What is strong coupling regime defined,
- In the non-resonant limit $\Delta \gg g$, how is the new Hamiltonian transformed from the JC model? What's the physical meaning of it.
- What is physical meaning of κ and γ of the system, how do they enter the equation of the system, and related to the measured cavity transmission and phase response in fig2?
- Why it's important to achieve strong coupling regime?
- What is the result they measured that indicate strong coupling?